HHS Public Access

Author manuscript

Oncogene. Author manuscript; available in PMC 2021 August 18.

Published in final edited form as:

Oncogene. 2021 March ; 40(10): 1909–1920. doi:10.1038/s41388-021-01668-x.

Cx43 phosphorylation sites regulate pancreatic cancer metastasis

Joell L. Solan[1,2], **Sunil R. Hingorani**[1,3], **Paul D. Lampe**[1,2,*]

[1]Translational Research Program, Public Health Sciences, Fred Hutchinson Cancer Research Center, Seattle WA 98109.

[2]Human Biology, Fred Hutchinson Cancer Research Center, Seattle WA 98109.

[3]Clinical Divisions, Fred Hutchinson Cancer Research Center, Seattle WA 98109.

Abstract

Pancreatic ductal adenocarcinoma (PDA) is aggressive, highly metastatic and characterized by a robust desmoplasia. Connexin proteins that form gap junctions have been implicated in tumor suppression for over 30 years. Cx43, the most widely expressed connexin, regulates cell behaviors, including migration and proliferation. Thus, we hypothesized that Cx43 could regulate PDA progression. Phosphorylation of Cx43 by Casein Kinase 1 (CK1) regulates gap junction assembly. We interbred the well-established $Kras^{LSL\text{-}G12D/+;p48Cre/+}$ (KC) mouse model of PDA with homozygous “knock-in” mutant Cx43 mice bearing amino acid substitution at CK1 sites ($Cx43^{CK1A}$) and found profound and surprising effects on cancer progression. Crossing the $Cx43^{CK1A}$ mouse onto the KC background (termed $KC;Cx^{CK1A}$) led to significant *extension of lifespan*, from a median of 370 to 486 days (p=0.03) and a decreased incidence of metastasis (p=0.045). However, when we examined early stages of disease, we found more *rapid onset* of tissue remodeling in the $KC;Cx^{CK1A}$ mouse followed by divergence to a cystic phenotype. During tumorigenesis, gap junctions are increasingly present in stromal cells of the KC mice but are absent from the $KC;Cx43^{CK1A}$ mice. Tail vein metastasis assays with cells derived from KC or $KC;Cx^{CK1A}$ tumors showed that $KC;Cx^{CK1A}$ cells could efficiently colonize the lung and downregulate Cx43 expression, arguing that inhibition of metastasis was not occurring at the distal site. Instead, stromal gap junctions, their associated signaling events or other unknown Cx43-dependent events facilitate metastatic capacity in the primary tumor.

Keywords

Pancreas cancer; Connexin; Gap Junction; phosphorylation

*To whom correspondence should be addressed: Paul Lampe, Translational Research Program, M5-C800, Fred Hutchinson Cancer Research Center, PO Box 19024, Seattle WA, 98109; plampe@fredhutch.org; Tel. (206) 667-4123.

Conflict of Interest

The authors declare they have no conflict of interest. PDL and JLS receive royalties from the sale of Cx43NT1 antibodies.

INTRODUCTION

Pancreas cancer or pancreatic ductal adenocarcinoma (PDA) is the third leading cause of cancer-related death in the United States with an annual mortality of ~47,000 people and 5-year overall survival rate of just 9% [1]. The extremely high mortality occurs primarily because symptoms do not present until tumors are locally unresectable and/or already metastatic. Even when surgical resection with clean margins in patients diagnosed at “early stages” is possible, almost inevitably lethal recurrence and metastatic disease result.

The interrelationship of gap junction biology and the regulation of tumor promotion, tumor progression and metastasis is well established and longstanding [2]. Gap junction plaques are specialized membrane domains made up of the connexin family of channel proteins, that allow intercellular exchange of small molecules (<1000 Da) including ions, metabolites, and second messengers (e.g., Ca^{2+} and IP_3) [3-5]. Studies on Cx43, the most widely expressed connexin (>34 tissues and 46 cell types [6]), clearly show that gap junction biology is highly regulated via Cx43 phosphorylation. Cx43 phosphorylation can modulate protein trafficking, stability of the junctional complex, gap junctional communication and interactions with other proteins [7-10]. In addition, gap junctions play an established role in wound healing and epithelial migration that involve dynamic changes in Cx43 localization and phosphorylation (e.g., [11]). Cx43 can affect cell behavior through at least 3 mechanisms: intercellular communication through channels, a cytoplasmic scaffold function provided by the gap junction plaque and as a conduit to the extracellular milieu via hemichannel opening. In the exocrine pancreas, acinar cells express primarily Cx26 and Cx32, ductal cells express Cx43 and Cx45 and pancreatic stellate cells express Cx43 [12, 13]. In pancreas tumor cells, Cx26 is retained while Cx32 and Cx43 decrease [14, 15] but Cx43 expression in stromal cells increases during cancer progression [16].

The mutational profile and histological progression of PDA are well defined; activating mutations in *KRAS* are found in over 90% of cases and are considered a driver of this cancer [17]. A robust desmoplasia is a critical feature of PDA and dynamic interactions between multiple cell types contribute to a complex tumor microenvironment and an inability to effectively treat these tumors [17]. Animal models of preinvasive and invasive PDA [17] have been generated through the targeted physiologic expression of oncogenic $Kras^{G12D}$ to the mouse pancreas (hereafter termed KC mouse). These models faithfully mimic the histology and genetics of human PDA.

Given the increase in Cx43 expression during PDA progression, we sought to test the effect of Cx43 phosphorylation on PDA progression. We hypothesized that a reduction in the efficiency of gap junction assembly would accelerate PDA progression. Thus, we interbred homozygous “knock-in” mutant Cx43 mice bearing amino acid substitutions at the 3 serines in the C-terminal tail region [18-20] phosphorylated by CK1 ($Cx43^{CK1A}$) into the KC mouse model of PDA. The $Cx43^{CK1A}$ mouse shows less efficient gap junction assembly [8, 20, 21] and *increased ERK1/2* activation in several tissues [21], features typically associated with tumorigenesis [22, 23]. Surprisingly, crossing the $Cx43^{CK1A}$ mouse onto the KC background (termed KC;Cx^{CK1A}) significantly *prolonged life*, decreased metastatic burden and shifted tumors to a *cystic phenotype*. However, the earliest stages of disease showed *more* rapid

progression to a preinvasive phenotype compared to the KC mouse. Thus, using an autochthonous *in vivo* model, we clearly show differential roles for Cx43 during tumor progression.

RESULTS

Mutation of Cx43 extends lifespan during PDA

Survival studies were performed to determine whether alteration of Cx43 phosphorylation could affect lifespan during PDA. $Cx43^{CK1A}$ and KC mice were interbred generating KC;Cx^{CK1A} animals at the expected ratios. A cohort of KC and KC;Cx^{CK1A} mice were maintained until requiring euthanasia due to poor health per established criteria (Materials and Methods). We saw that the Cx43 mutation extended survival by 30% (median survival KC: 370 days vs KC;Cx^{CK1A}: 486 days, p=0.03 by log rank). The survival curves revealed that both KC and KC;Cx^{CK1A} genotypes showed similar survival in the first quartile; the curves begin to separate at ~310 days as KC mice rapidly succumb to disease (Fig. 1A). Histopathological analysis upon death showed that all animals had primary pancreatic cancer. In the absence of activated Kras there was no statistical difference in survival between WT and $Cx43^{CK1A}$ mice with mortality beginning at ~530 days (Fig. 1A, dotted line). At this time 90% of KC mice have succumbed while 50% of KC;Cx^{CK1A} mice are still alive, emphasizing the protection from PDA conferred by the KC;Cx^{CK1A} cross.

KC;Cx^{CK1A} mice have diminished metastatic disease burden

KC mice had a higher prevalence of macroscopic metastases than KC;Cx^{CK1A} mice (12/19 vs. 9/24, Fig. 1B). We saw a similar tropism for metastases in both genotypes with most occurring in the liver and occasionally the lung (Supplemental Fig. 1). The number of metastases in the KC mice, in particular, may be undercounted as 4 KC and 1 KC;Cx^{CK1A} mice were found dead, precluding tissue analyses. Histological analysis showed that nearly half of the KC;Cx^{CK1A} metastases were not from PDA, instead, 2 were identified as primary sarcomas and 2 as hematopoietic neoplasms. Only 2 metastases in KC mice were not of PDA origin, identified, instead, as an osteosarcoma and a hematopoietic neoplasm (“other” in Fig. 1B, Supplemental Fig. 1). The majority of PDA metastases showed a glandular phenotype regardless of genotype. Thus, KC;Cx^{CK1A} mice had a lower incidence of metastatic PDA ($p<0.05$ by Fisher’s exact test comparing histologically confirmed PDA metastases), consistent with the extended lifespan of this genotype.

Next, we examined Cx43 expression in metastases to determine a potential role for gap junctions in this process. We saw very little Cx43 expression in liver metastases from either genotype with 5 of 7 KC mice showing no Cx43 (Fig. 1F) and the other 2 showing only sporadic, limited positive staining in 2 very large metastases and none in small metastases (Fig. 1C-E). We also stained 2 lung metastases from KC mice, which were negative for Cx43 (Supplemental Fig. 1A-C). 4 of 5 KC;Cx^{CK1A} metastases showed no Cx43 staining, although one had extensive staining. This lack of Cx43 expression at the metastatic site indicated that Cx43 was not playing a necessary role in either initiation or growth of metastases.

Cx43 phosphorylation regulates tumor progression at early stages

To quantify rates of disease progression, mice were randomized to 6, 12 and 16-month timepoints and analyzed by necropsy and histology (n=10/genotype/timepoint). We developed a histological classifier to identify acinar cells in hematoxylin and eosin (H&E) stained tissues (Supplemental Fig. 2) and found (Fig. 2A) an almost complete loss of the normal acinar parenchyma in KC;Cx^{CK1A} pancreata (5.08±1.42% remaining) while KC mice maintained over 20% of the normal parenchyma (22.5±4.5%,p=0.007). Conversely, staining with Alcian Blue, which stains mucin found in pancreatic intraepithelial neoplasias (PanINs), was increased in KC;Cx^{CK1A} mice (5.4± 1.8%KC;Cx^{CK1A} vs 2.5±0.9% KC, p=0.05; Fig. 2A). To determine whether this was due to faster progression or earlier onset, we performed H&E staining on pancreata from 3-month-old KC;Cx^{CK1A} and C;Cx^{CK1A} animals and saw predominantly acinar cell staining arguing against earlier onset of dedifferentiation (Supplemental Fig. 3). This difference did not seem to involve increased proliferation as staining with Ki67 showed no statistical difference in KC vs KC;Cx^{CK1A} pancreata across tissue compartments (i.e., acinar, stromal or PanIN) (Supplemental Fig. 3). Thus, Cx43 phosphorylation plays a regulatory role in modulating cell fate through acceleration, but not onset, of acinar-to-ductal metaplasia (ADM).

Cx43 regulates signaling pathways involved in PDA progression

Further evidence for altered cell fate was suggested by a dramatic change in the phenotype of the pancreata in 16-month mice. KC pancreata at this age contained large, dense nodules typical of PDA [24] while most of the KC;Cx^{CK1A} mice had large, often multi-compartmental cysts (Fig. 2B, 8/10 KC;Cx^{CK1A} vs. 2/10 KC animals, p=0.023, Fisher's exact test). Cystic phenotypes, known to occur in both mouse and human PDA [25], can be distinguished as intraductal papillary mucinous neoplasms (IPMN) or mucinous cystic neoplasms (MCN). MCNs are histologically defined as having an "ovarian stroma" in which fibroblasts stain positive for estrogen and progesterone receptor surrounding the cyst. KC;Cx^{CK1A} cysts showed an ovarian stroma and progesterone receptor staining in some areas, consistent with a MCN diagnosis, though it was not always closely associated with the cyst (Fig. 2C).

Cx43 phosphorylation regulates metastasis at the primary tumor site

The $Cx43^{CK1}$ mice express mutant Cx43 constitutively (i.e., throughout the mouse) while $Kras^{G12D}$ expression is limited primarily to the pancreas; thus Cx43 expression could be influencing the ability of the tumor cell to escape the primary tumor through tumor cell-autonomous mechanisms, via heterologous interactions with other cells and/or through effects altering the metastatic niche rendering it inhospitable to tumor seeding/growth. To better understand the Cx43:metastasis relationship, we generated primary tumor cell lines from both KC and KC;Cx^{CK1A} pancreas tumors and performed tail vein metastasis assays using a "seed" vs "soil" experimental design. The KC and KC;Cx^{CK1A} primary tumor cells acted as "seed" and were injected into the tail vein of either immune deficient (NOD/SCID) mice or immunocompetent mice expressing WT or CK1A mutant Cx43; we then assessed their ability to colonize and grow in the lungs of these animals, which behaved as the "soil" (Fig. 3). Note that immune competent recipient mice expressed $Kras^{G12D}$ but not $p48^{Cre}$ so

activated Kras was not present to confound the results. Mice were injected with $5x10^5$ cells. Immune competent animals were sacrificed after 2 weeks to analyze lungs by histology. NOD/SCID mice began showing signs of distress and were sacrificed at 10 days. We performed H&E staining on lungs and developed a tissue classifier to distinguish tumor cells from normal lung. The ability to colonize lungs seemed to reside entirely with the "seed", as KC;Cx^{CK1A} tumor cells comprised more than 60% of lung tissue area in recipients (regardless of genotype) while KC tumor cells comprised only about 40% of area in all recipients (Fig. 3A and Supplemental Fig. 4). Thus, the CK1A site mutations did not diminish the capacity of the lungs to be colonized. Instead KC;Cx^{CK1A} cells appeared to have a colonization advantage.

We examined Cx43 expression in the lungs and found that, in immunocompetent mice, KC donor cells expressed higher levels of Cx43 than KC;Cx^{CK1A} donor cells (Fig. 3B). This is consistent with KC;Cx^{CK1A} cells having less stable gap junctions [19, 21] as the tumor microenvironment is typically destabilizing for epithelial gap junctions [2, 26]. Staining the lung tumor tissue with PCNA showed no obvious proliferative advantage for KC;Cx^{CK1A} cells (KC:KC 26.8±6.4%, KC;Cx^{CK1A}:KC 24.3±1.7%, KC;Cx^{CK1A}:nude 28.3±4.1% nuclei positive for PCNA; Supplementary Fig. 5). These data, combined with the lack of proliferative changes at 6 months (Supplementary Fig. 3), indicate that changes in proliferation are not a dominant effect of Cx43 during pancreatic tumorigenesis.

Analysis of Cx43 expression in nude mice led to the surprising finding that the immune system might be playing a role in regulating Cx43 expression; we found that in nude mice neither KC nor KC;Cx^{CK1A} cells expressed Cx43 in the lung even though the cell lines injected were positive for Cx43 *in vitro*. We examined primary cell lines isolated from tumors from 2 different mice of each genotype (4 in total) (KC cell line 1 derived from mouse #4522; KC cell line 2 from mouse #1908; KC;Cx^{CK1A} cell culture 1 from mouse #1128 and KC;Cx^{CK1A} cell culture 2 from mouse #3450; Cell culture 1 was used for tail vein injections) and saw Cx43 expression by both immunofluorescence (Fig. 4A) and immunoblot (Fig. 4B). While Cx43 levels trended higher in KC;Cx^{CK1A} cells this did not reach significance (KC;Cx^{CK1A} cell line 1=0.71 ±0.48, KC;Cx^{CK1A} cell line 2=0.68±0.37 vs KC cell line 1=1.30±0.38, KC cell line 2 =1.08±0.15 a.u., p=0.09). Thus, the immune system was able to support Cx43 expression in KC cells but not in KC;Cx^{CK1A} cells.

KC;Cx^{CK1A} mutation promotes an epithelial phenotype

We also observed a phenotypic difference where the injected KC;Cx^{CK1A} cells appeared to be more differentiated (Fig. 3 and Supplemental Fig. 3). One possibility is that the glandular phenotype of the KC;Cx^{CK1A} cells reflected a more differentiated or epithelial cell state. To address this possibility, we analyzed 2 primary tumor cell lines of each genotype by immunoblot. Indeed, we found that both KC;Cx^{CK1A} tumor cell lines expressed over 5 times as much E-Cadherin as the 2 KC tumor cell lines (Fig. 4B, KC;Cx^{CK1A} cell line 1=0.91 ±0.10, KC;Cx^{CK1A} cell line 2=0.67±0.18 vs KC cell line 1=0.13±0.05, KC cell line 2 =0.04±0.01 a.u. p=0.03). Thus, KC cells appear to have a more EMT phenotype, which is consistent with more metastatic potential.

Signaling through ERK1/2 and Akt have been shown to be activated in PDA [27, 28], and the CK1A mutation can increase phospho-ERK1/ levels [21]. However, Cx43 mutation did not appear to consistently alter the levels or phosphorylation status of these signaling molecules in these primary tumor cells (Supplementary Fig. 6). We recently showed that CK1A mutation more than doubled NDRG1 expression in heart tissue and cell lines while the CK1E mutant, mimicking phosphorylation, diminished expression [21]. NDRG1 has been shown to be a metastasis suppressor in pancreatic and other cancers [29, 30]. Indeed, immunoblotting for NDRG1 in the primary tumor cell lines recapitulated this effect showing NDRG1 levels nearly 5 times higher in KC;Cx^{CK1A} animals compared to KC (Fig. 4B, $p<0.003$). Finally, we have previously shown that in non-transformed cells the CK1A mutation inhibits migration in a scratch wound assay [8]. Thus, increased E-Cadherin combined with elevated NDRG1 expression in the KC;Cx^{CK1A} primary tumor cells indicates that these cells are better able to maintain an epithelial identity than cells from KC mice and is consistent with a model where inhibition of metastasis in KC;Cx^{CK1A} mice is occurring at the site of the primary tumor.

Gap junction plaques are more common in KC compared to KC;Cx^{CK1A} mice

We previously reported that Cx43 expression increased during pancreas tumor progression [16]. We performed immunoblots on primary tumor lysates for both genotypes and did not see a consistent change in Cx43 or NDRG1 expression (Supplemental Fig.7A and B). However, the variability in expression was quite high across animals, and we know pancreatic tumor tissue is quite heterogenous. When we examined primary tumor tissue by IHC we continued to see high variability for NDRG1 staining (Supplemental Fig. 7C). Cx43 staining showed regional variation, with some areas exhibiting many positive cells, while neighboring areas with similar histology were negative (Supplemental Fig. 8). However, we saw a distinct difference in Cx43 staining in KC vs KC;Cx^{CK1A} tissue where KC mice exhibited punctate Cx43 staining, consistent with assembly of gap junction plaques while staining in KC;Cx^{CK1A} tissue appeared more cytoplasmic (Fig. 5). To compare Cx43 expression in KC vs KC;Cx^{CK1A} mice, 5 blinded, independent reviewers scored the extent of Cx43 expression as 0, 1 or 2 in “punctate” (typical for Cx43 present in gap junctions) or “cytoplasmic” categories. Fig. 5 shows that KC animals scored more highly for punctate staining (mean score for KC=1.69 vs. KC;Cx^{CK1A}=0.64, $p=0.002$) and, conversely, KC;Cx^{CK1A} animals scored higher for cytoplasmic staining (mean score for KC=1.05 vs. KC;Cx^{CK1A}=1.71, $p<0.001$, IHC controls and data for individual animals in Supplemental Fig. 9). As we reported previously in KC animals [16], Cx43 expression was highest in the stroma surrounding areas with advanced PanINs and carcinoma *in situ*; however, it was excluded from areas where the tumor cells were dense and dedifferentiated. Cx43 staining in KC;Cx^{CK1A} pancreata could also be found in the stroma but staining was less common. Somewhat surprisingly, we did not see staining in PanINs, in spite of the fact that primary tumor cells were Cx43 positive (Fig.4). We also performed IHC for Cx43 on pancreata from old C; Cx^{CK1A} and p48Cre expressing animals (i.e. without PDA) which contained predominantly acinar cells and did not observe any Cx43 staining, arguing that Cx43 expressing cells resulted from tumorigenesis and not age (Supplemental Fig. 9).

Cancer associated fibroblasts interact via gap junctions

Fig. 6B,D,F,H and I-L show IHC and immunofluorescence examples of Cx43 staining in pancreas tissue from moribund mice. Fig. 6A and E show vimentin staining. Fig. 6A,B and 6C,D serial sections show cells closely associated with the basolateral boundaries of PanINs (arrowheads) while Fig. 6E,F and 6G,H show Cx43 expressing cells in the stroma. IHC staining of serial sections for vimentin indicate a mesenchymal origin for these cells (Fig. 6A) while CK19 staining (a marker of PDA epithelia) did not show consistent localization of Cx43 in tumor epithelia (Fig. 6C,6G and Supplemental Fig. 10C,D,E). In addition, supplemental Fig. 10A and 10B serial sections stained with Masson's Trichrome (collagen) show that Cx43 expression appears to localize to areas with high matrix deposition levels. Finally, staining with the immune cell marker CD45 and the endothelial marker CD31 did not coincide with Cx43 staining (Supplemental Fig. 10G-J). These data are consistent with Cx43 being predominantly expressed in fibroblasts. Activated fibroblasts are prominent in pancreas cancers [31] and "cancer associated fibroblasts" (CAF) are an active area of investigation [32]. In PDA, at least 2 categories of fibroblasts have been described, largely distinguished by expression of either smooth muscle actin (SMA^+) or fibroblast activation protein-α ($FAP\alpha^+$) [33, 34]. We performed multiplex immunofluorescent staining of PDA tissue to determine whether Cx43 segregated to one of these fibroblast compartments. Staining with cytokeratin 19 (Fig. 6C,G CK19 in red), which marks tumor derived epithelial cells and SMA (green) showed that cells making gap junctions (Cx43 in white, arrowheads) were commonly positive for SMA and negative for CK19. SMA positivity was especially apparent when gap junctions were seen in very close association with epithelial cells that maintained a ductal structure (Fig 6C). As gap junction expression became more stromal, we began to see less consistent association with SMA. Multiplex staining with Cx43 (white), FAPα (red) and SMA (green) show that junctions could be found in a variety of stromal cells including those expressing only SMA (green arrowheads), only FAPα (red arrowheads), both (yellow arrowheads) or neither (white arrowheads) (Figure 6, panels I-L). Again, Cx43 was not expressed homogenously throughout the tissue but instead showed regional variations in intensity (Supplemental Fig. 8) indicating that gap junction stability is regulated or induced in response to local cues that create a potential stromal communication compartment or a Cx43-dependent signaling scaffold. The lack of punctate Cx43 staining in KC;Cx^{CK1A} tumors (Fig. 5) supports the hypothesis that gap junctions are contributing to a microenvironment that supports metastasis.

Discussion

In our study, the most dramatic effect of eliminating Cx43 phosphorylation by CK1 was the extended lifespan in the KC;Cx^{CK1A} mice. Metastatic burden is the ultimate cause of death for most solid tumors and, indeed, we saw decreased metastases in these animals. Metastasis is a complex process requiring dynamic rearrangement of tissue architecture both at the primary tumor and metastatic sites [35]. To determine where Cx43 phosphorylation might control the metastatic process, we performed tail vein metastasis assays to test the ability of tumor cells to extravasate and grow ("seed") at the metastatic site ("soil"), in this case the lung. We found that the ability of cells to colonize and grow in the lung segregated entirely with the genotype of the "seed" ruling out a major impact of the "soil" in colonization (Fig.

3). This was further supported by the lack of Cx43 expression in metastases to both the liver and lung (Fig. 1). These data indicate inhibition of metastasis was occurring at the primary tumor site.

While both KC and KC;Cx^{CK1A} animals developed extensive primary PDA, Cx43 expression and localization were distinct in each genotype. In KC animals, IHC with multiple markers indicate CAFs sporadically made gap junctions in areas that retained glandular architecture but not in advanced carcinomas. Dynamic regulation of fibroblasts is an area of increasing interest as a target for intervention in cancer [32, 36-38]. In PDA, at least 2 overlapping categories of CAFs are described, SMA^+ which appear to be protective [39] and $FAP\alpha^+$ which promote tumorigenesis [34, 40] . Similarly, in established models of vascular remodeling and epidermal wounding, fibroblasts can undergo phenotype switching from a contractile or myofibroblast phenotype (SMA^+) to a synthetic phenotype involved in matrix deposition and PDGF signaling [41, 42] similar to the $FAP\alpha^+$ phenotype [40]. There is also recent evidence for a CAF population in PDA that develops in response to IL-1β and promotes inflammation (iCAFs) [43]. Interestingly, Cx43 hemichannels have been shown to promote IL-1β secretion through activation of the NLRP3 inflammosome [44] and NLRP3 appears to promote PDA [45]. A role for Cx43 in phenotype switching has been shown by several groups with Cx43 supporting the synthetic phenotype. In models of vascular injury, knockdown of Cx43 or inhibition of gap junction communication (GJC) shifted smooth muscle cells to a myofibroblast phenotype [41, 46]. A similar role for Cx43 in cultured human activated pancreatic stellate cells was also shown where inhibition of GJC shifted cells to the myofibroblast phenotype while quiescent rat pancreatic stellate cells required GJC to differentiate to the myofibroblast phenotype [12]. Thus, Cx43 could be playing a pro-tumorigenic role through effects on fibroblasts in PDA. In our in vivo system, however, we observed Cx43 in fibroblasts in various states indicating more complicated regulation.

In addition to the cellular complexity of PDA tumors, they are sites of incredibly high interstitial pressure as a result of the extracellular matrix secreted by CAFs [47]. Cx43 is mechanosensitive and often increased in response to mechanical load [48]; thus, biophysical cues could be driving local expression of Cx43. Another possibility is that cells making gap junctions could be recruiting or helping retain specific cell types that contribute to remodeling of the tumor microenvironment. A role for gap junctions in recruitment of alveolar macrophages via interaction with alveolar type 2 epithelial cells was shown in a *Keap1*-deficient $Kras^{G12D}$ model of lung cancer [49]. We observed that the KC;Cx^{CK1A} model lacked gap junctions in the tumor microenvironment, had less metastases and yielded primary tumor cells that maintained an epithelial phenotype, arguing that these cells evolved in a different tumor microenvironment. Whether this was mediated through gap junction channel and/or scaffold functions is difficult to address *in vivo.* However, our data argue that gap junctions in the stroma can regulate the tumor microenvironment and promote transition to a metastatic phenotype.

The time course studies showed that the KC;Cx^{CK1A} model accelerated the transition from normal parenchyma to the preinvasive phenotype consistent with our original hypothesis. Activated Kras appears to drive acinar cells through a dedifferentiation program that gives rise to PanINs and ultimately PDA, a distinct and necessary step in progression to PDA

referred to as acinar ductal metaplasia (ADM) PDA [50]. Though Cx43 expression was low in these early stages, it was recently shown that gap junctions play an important role in promoting early pancreatic development [51]. While KC;Cx^{CK1A} animals appeared to develop normal pancreata, even at 3 months, destabilization of gap junctions during development may have resulted in an underlying indolence that predisposed mature pancreatic cells to dedifferentiation thus explaining the rapid onset of ADM observed.

Alteration of signaling and cell fate was also indicated by divergence of the KC;Cx^{CK1A} animals to a cystic, possibly MCN, phenotype. Other examples of $Kras^{G12D}$ compound mutants giving rise to the MCN phenotype have been reported including a NOTCH2 knockout [52], mutants that constitutively stabilize HIF2α [53] and Smad4/Dpc4 heterozygous and homozygous deletions [54]. The NOTCH2 knockout shows an extended lifespan but does not progress to pancreatic cancer via PanIN progression instead giving rise to an anaplastic malignant transformation characterized by a strong EMT phenotype. Loss of Smad4 is a known genetic feature that typically occurs in advanced PDA, but Izeradjene, et al. showed that early SMAD4 haploinsufficiency could alter the histopathologic course of disease (i.e., towards an MCN phenotype) with a decreased proliferative capacity as they developed PDA with a similar lifespan albeit decreased metastatic burden compared to KC animals [54]. These models are distinct from the KC;Cx^{CK1A} phenotype reported here, where we observed extended lifespan and decreased metastasis. Thus, as observed in the conventional PanIN-to-PDA scheme, multiple pathways to a cystic phenotype are suggested by these models and are likely influenced by the hetero-cellular interactions that are a hallmark of all PDAs.

Elimination of CK1 phosphorylation sites on Cx43 leads to stabilization of NDRG1 [21]. NDRG1 has been shown to be correlated with better prognoses in pancreatic cancer through an ability to inhibit migration and invasion [29]. Another study on human PDA showed that NDRG1 was highly expressed in well-differentiated cells and absent from poorly differentiated tumor cells [30]. This pattern is again consistent with KC;Cx^{CK1A} tumor cells maintaining an epithelial phenotype and reduced metastases in these animals.

Our experiments argue that gap junctions between stromal CAFs support a microenvironment that can enhance metastasis through regulation of EMT and/or through effects on tumor cell escape from the primary site. The in vitro work from other labs showing that gap junctions can shift cells to a secretory phenotype [12, 41, 46] argues that Cx43 could, indeed, be modulating the phenotype of CAFs *in vivo*. If this were the case, targeting of Cx43 could have broad effects on the fibrotic or immune profile of these tumors. A role for stromal gap junctions in mediating tumor cell adhesion and invasion has been suggested in other studies [55, 56] indicating that Cx43 expressing CAFs may prove to be an important player not just in PDA but other types of cancer.

Though much is known about the genetic drivers of PDA, this disease continues to be resistant to therapy, in large part, due to a dynamic and complex tumor architecture and microenvironment that evolves through the interplay of multiple cell types over time [47]. Interestingly, epidermal wounding also requires a dynamic and coordinated response involving similar cell types and functions, and the idea of cancer as a wound that won’t heal

has been suggested by multiple groups (e.g., [57]). We and others have shown that Cx43 phosphorylation is also dynamically regulated during wound healing [8, 10, 11]. Indeed, genetic modulation of different Cx43 phosphorylation sites has the opposite effect on wound healing; the $Cx43^{CK1A}$ mouse healed wounds more slowly, while elimination of MAPK phosphorylation sites ($Cx43^{MAPKA}$ mouse) caused faster healing [8, 11]. Furthermore, a drug that modulates Cx43 expression shows promise in promoting wound healing and is currently in phase 3 clinical trials [58]. Here, we showed that regulation of Cx43 in PDA can also have dramatic effects on outcome and could be a potential therapeutic target.

Materials and Methods

Reagents and antibodies:

All general chemicals, unless noted, were from Thermo Fisher Scientific (Waltham, MA). Antibodies used for immunoblotting: anti-Cx43, Cx43NT1 made at the Fred Hutchinson Cancer Research Center Antibody Technology Facility (Seattle, WA); E-cadherin, #3195 Cell Signaling Technology (Danvers, MA); NDRG1, Vimentin, #13901 Cell Signaling Technology; Vinculin V4505 MilllporeSigma (Burlington, MA); Immunohistochemistry: Cx43 (6219, MilliporeSigma); Ki67 (12202 Cell Signaling Technology), Progesterone receptor (Lab Vision SP2, Thermo Fisher), Vimentin (Novus Biologicals, Centennial, CO); Immunofluorescence: anti-PCNA (NA03, MilliporeSigma), CK19 (TROMA-3 Developmental Studies Hybridoma Bank (Iowa City, IA)), smooth muscle actin (A5228 MiliporeSigma). Secondary antibodies from ThermoFisher: Rat IgG 647 (A21247); anti-rabbit IgG 594 (A32754); anti-mouse IgG2a 488 (A32723).

Mouse strains and tissue processing:

All mouse studies were conducted with Institutional Animal Care and Use Committee approval (IACUC). $Cx43^{CK1}$ [59] and KC [17] mice were generated as previously described and inbred into a C57Bl6/6J strain background. For survival studies, animals were bred until at least 22 animals of each genotype were born (per power calculation with 30% effect) and monitored per IACUC-approved rodent tumor monitoring standard operating procedures. Briefly, mice were monitored 3 times weekly until a palpable tumor was evident, then daily until euthanasia was advised due to signs of distress including (but not limited to) respiratory or mobility problems. Animals underwent necropsy and tissue was formalin-fixed or flash frozen as previously described [60]. Entry into time-course cohorts was randomized so that animals were entered into predetermined positions at birth, then euthanized at the appropriate age (or earlier, if advised), necropsied and tissue collected.

Histochemistry and Immunohistochemistry:

Sections (4μm) of formalin-fixed, paraffin-embedded tissues were deparaffinized with xylene and rehydrated. Serial sections were stained with H&E or Alcian Blue as described [17]. Immunohistochemistry was performed on a Leica BOND autostainer (Wetzlar, Germany). Slides were scanned in brightfield using the Aperio Digital Pathology System (Leica). Images were analyzed using the Tissue Classifier and Area Quantification modules of the HALO Image Analysis System v.3.0 (Indica labs, Albuquerque, NM). For immunofluorescence antigen retrieval was performed in a pressure cooker using 10mM

Sodium citrate, pH 6.0. Primary antibodies were incubated overnight followed by incubation with secondary antibodies and TrueVIEW (SP-8400, Vector Laboratories, Burlingame, CA). Images were captured with a Nikon DSVi1 brightfield camera using NIS Elements 3.2 Basic Research Image software (Nikon Instruments Inc., Melville, NY).

Immunoblotting:

Flash frozen pancreata were homogenized in Laemmli Sample buffer containing 1x Complete protease inhibitor cocktail, 1x phosphatase inhibitor cocktail and 2mM Phenylmethylsulfonyl fluoride (all from MilliporeSigma) using a glass pestle tissue grinder. Primary cell lysates were directly lysed in Laemmli Sample Buffer containing the same inhibitors. After sonication samples were separated by SDS-PAGE, blotted to nitrocellulose, checked for load with Ponceau S, blocked in 1% milk and probed with antibodies as noted. Antibodies were detected with appropriate secondary antibodies conjugated to AlexaFluor680 or AlexaFlour790 (Thermo Fisher Scientific) and directly quantified using the Li-Cor Biosciences Odyssey infrared imaging system and associated software (Lincoln, NE). Normalized densitometry values were calculated as a ratio to vinculin (chosen as loading control as it showed high correspondence with Ponceau S staining in previous experiments).

Tail vein injections

were performed by our Co-operative Center for Excellence in Hematology per IACUC approved Standard Operating Procedures. Briefly, 0.2ml of warm PBS containing 0.5 x 10^6 cells derived from KC or KC;Cx^{CK1A} tumors were injected into either NOD/SCID, $Kras^{G12D}$ or $Kras^{G12D}$;Cx^{CK1A} mice. Animals were monitored every 5 days; immune competent animals were euthanized after 2 weeks while NOD/SCID mice began showing signs of distress and were euthanized at 10 days. Necropsies were performed and tissue was collected.

All graphs show mean and standard deviation, further information on statistics can be found in Supplemental Figure 11.

Supplementary Material

Refer to Web version on PubMed Central for supplementary material.

Acknowledgements

H & E pathology analysis was performed by Sue Knoblaugh, DVM, Diplomate ACVP. Yutaka Yasui, PhD performed power calculations and aided in the experimental design of the mouse experiments. This work was supported by grants R21CA149554 and GM55632 from the National Institutes of Health. The content is solely the responsibility of the authors and does not necessarily represent the official views of the National Institutes of Health.

Abbreviations:

Cx	connexin
GJC	gap junction communication

PDA	pancreatic adenocarcinoma
KC	$Kras^{G12D}$
WT	wild type
DAPI	4’,6 diamidine-2-phenylindole
H & E	hematoxylin and eosin
PanIN	pancreatic intraepithelial neoplasm
CK1	casein kinase 1
ERK	extracellular signal-related kinase
CK19	cytokeratin 19
SMA	smooth muscle actin
ADM	acinar ductal metaplasia
CAF	cancer-associated fibroblast
MCN	mucinous cystic neoplasm
EMT	epidermal to mesenchymal transition
IHC	immunohistochemistry
FFPE	formalin-fixed, paraffin-embedded
NDRG1	N-Myc Downstream Regulated 1

References

1. American Cancer Society. Cancer Statistics Center. In: https://cancerstatisticscenter.cancer.org (ed), 2020.
2. Aasen T, Mesnil M, Naus CC, Lampe PD, Laird DW. Gap junctions and cancer: communicating for 50 years. Nat Rev Cancer 2016; 16: 775–788. [PubMed: 27782134]
3. Loewenstein WR. Junctional intercellular communication: The cell-to-cell membrane channel. Physiol Rev 1981; 61: 829–913. [PubMed: 6270711]
4. Willecke K, Eiberger J, Degen J, Eckardt D, Romualdi A, Guldenagel M et al. Structural and functional diversity of connexin genes in the mouse and human genome. Biol Chem 2002; 383: 725–737. [PubMed: 12108537]
5. Saez JC, Berthoud VM, Branes MC, Martinez AD, Beyer EC. Plasma membrane channels formed by connexins: their regulation and functions. Physiol Rev 2003; 83: 1359–1400. [PubMed: 14506308]
6. Laird DW. Life cycle of connexins in health and disease. Biochem J 2006; 394: 527–543. [PubMed: 16492141]
7. Solan JL, Lampe PD. Connexin43 phosphorylation: structural changes and biological effects. Biochem J 2009; 419: 261–272. [PubMed: 19309313]
8. Lastwika KJ, Dunn CA, Solan JL, Lampe PD. Phosphorylation of connexin 43 at MAPK, PKC or CK1 sites each distinctly alter the kinetics of epidermal wound repair. J Cell Sci 2019; 132.

9. Solan JL, Lampe PD. Specific Cx43 phosphorylation events regulate gap junction turnover in vivo. FEBS Lett 2014; 588: 1423–1429. [PubMed: 24508467]
10. Solan JL, Lampe PD. Kinase programs spatiotemporally regulate gap junction assembly and disassembly: Effects on wound repair. Semin Cell Dev Biol 2016; 50: 40–48. [PubMed: 26706150]
11. Richards TS, Dunn CA, Carter WG, Usui ML, Olerud JE, Lampe PD. Protein kinase C spatially and temporally regulates gap junctional communication during human wound repair via phosphorylation of connexin43 on serine368. J Cell Biol 2004; 167: 555–562. [PubMed: 15534005]
12. Masamune A, Suzuki N, Kikuta K, Ariga H, Hayashi S, Takikawa T et al. Connexins regulate cell functions in pancreatic stellate cells. Pancreas 2013; 42: 308–316. [PubMed: 22889984]
13. Cigliola V, Allagnat F, Berchtold LA, Lamprianou S, Haefliger JA, Meda P. Role of Connexins and Pannexins in the Pancreas. Pancreas 2015; 44: 1234–1244. [PubMed: 26465951]
14. Garcia-Rodriguez L, Perez-Torras S, Carrio M, Cascante A, Garcia-Ribas I, Mazo A et al. Connexin-26 is a key factor mediating gemcitabine bystander effect. Mol Cancer Ther 2011; 10: 505–517. [PubMed: 21388975]
15. Kyo N, Yamamoto H, Takeda Y, Ezumi K, Ngan CY, Terayama M et al. Overexpression of connexin 26 in carcinoma of the pancreas. Oncol Rep 2008; 19: 627–631. [PubMed: 18288393]
16. Solan JL, Hingorani SR, Lampe PD. Changes in connexin43 expression and localization during pancreatic cancer progression. J Membr Biol (Research Support, N.I.H., Extramural) 2012; 245: 255–262.
17. Hingorani SR, Petricoin EF, Maitra A, Rajapakse V, King C, Jacobetz MA et al. Preinvasive and invasive ductal pancreatic cancer and its early detection in the mouse. Cancer Cell 2003; 4: 437–450. [PubMed: 14706336]
18. Cooper CD, Lampe PD. Casein kinase 1 regulates connexin43 gap junction assembly. J Biol Chem 2002; 277: 44962–44968. [PubMed: 12270943]
19. Lampe PD, Cooper CD, King TJ, Burt JM. Analysis of Connexin43 phosphorylated at S325, S328 and S330 in normoxic and ischemic heart. J Cell Sci 2006; 119: 3435–3442. [PubMed: 16882687]
20. Remo BF, Qu J, Volpicelli FM, Giovannone S, Shin D, Lader J et al. Phosphatase-Resistant Gap Junctions Inhibit Pathological Remodeling and Prevent Arrhythmias. Circ Res 2011; 108: 1459–1466. [PubMed: 21527737]
21. Solan JL, Marquez-Rosado L, Lampe PD. Cx43 phosphorylation mediated effects on ERK and Akt protect against ischemia reperfusion injury and alter stability of stress-inducible protein NDRG1. J Biol Chem 2019.
22. King TJ, Gurley KE, Prunty J, Shin JL, Kemp CJ, Lampe PD. Deficiency in the gap junction protein connexin32 alters p27Kip1 tumor suppression and MAPK activation in a tissue-specific manner. Oncogene 2005; 24: 1718–1726. [PubMed: 15608667]
23. Trosko JE, Chang CC, Madhukar BV, Klaunig JE. Chemical, oncogene, and growth factor inhibition of gap junctional intercellular communication: an integrative hypothesis of carcinogenesis. Pathobiol 1990; 58: 265–278.
24. Chu GC, Kimmelman AC, Hezel AF, DePinho RA. Stromal biology of pancreatic cancer. J Cell Biochem 2007; 101: 887–907. [PubMed: 17266048]
25. Maitra A, Fukushima N, Takaori K, Hruban RH. Precursors to invasive pancreatic cancer. Adv Anat Pathol 2005; 12: 81–91. [PubMed: 15731576]
26. King TJ, Lampe PD. Temporal regulation of connexin phosphorylation in embryonic and adult tissues. Biochim Biophys Acta 2005; 1719: 24–35. [PubMed: 16137642]
27. Eser S, Schnieke A, Schneider G, Saur D. Oncogenic KRAS signalling in pancreatic cancer. Br J Cancer 2014; 111: 817–822. [PubMed: 24755884]
28. Mann KM, Ying H, Juan J, Jenkins NA, Copeland NG. KRAS-related proteins in pancreatic cancer. Pharmacol Ther 2016; 168: 29–42. [PubMed: 27595930]
29. Cen G, Zhang K, Cao J, Qiu Z. Downregulation of the N-myc downstream regulated gene 1 is related to enhanced proliferation, invasion and migration of pancreatic cancer. Oncol Rep 2017; 37: 1189–1195. [PubMed: 28075464]

30. Angst E, Sibold S, Tiffon C, Weimann R, Gloor B, Candinas D et al. Cellular differentiation determines the expression of the hypoxia-inducible protein NDRG1 in pancreatic cancer. Br J Cancer 2006; 95: 307–313. [PubMed: 16832411]
31. Yen TW, Aardal NP, Bronner MP, Thorning DR, Savard CE, Lee SP et al. Myofibroblasts are responsible for the desmoplastic reaction surrounding human pancreatic carcinomas. Surgery 2002; 131: 129–134. [PubMed: 11854689]
32. Sahai E, Astsaturov I, Cukierman E, DeNardo DG, Egeblad M, Evans RM et al. A framework for advancing our understanding of cancer-associated fibroblasts. Nat Rev Cancer 2020; 20: 174–186. [PubMed: 31980749]
33. Whittle MC, Hingorani SR. Fibroblasts in Pancreatic Ductal Adenocarcinoma: Biological Mechanisms and Therapeutic Targets. Gastroenterology 2019; 156: 2085–2096. [PubMed: 30721663]
34. Lo A, Li CP, Buza EL, Blomberg R, Govindaraju P, Avery D et al. Fibroblast activation protein augments progression and metastasis of pancreatic ductal adenocarcinoma. JCI Insight 2017; 2.
35. Hanahan D, Weinberg RA. Hallmarks of cancer: the next generation. Cell 2011; 144: 646–674. [PubMed: 21376230]
36. Vickman RE, Faget DV, Beachy P, Beebe D, Bhowmick NA, Cukierman E et al. Deconstructing tumor heterogeneity: the stromal perspective. Oncotarget 2020; 11: 3621–3632. [PubMed: 33088423]
37. Helms E, Onate MK, Sherman MH. Fibroblast Heterogeneity in the Pancreatic Tumor Microenvironment. Cancer Discov 2020; 10: 648–656. [PubMed: 32014869]
38. Chen X, Song E. Turning foes to friends: targeting cancer-associated fibroblasts. Nat Rev Drug Discov 2019; 18: 99–115. [PubMed: 30470818]
39. Ozdemir BC, Pentcheva-Hoang T, Carstens JL, Zheng X, Wu CC, Simpson TR et al. Depletion of carcinoma-associated fibroblasts and fibrosis induces immunosuppression and accelerates pancreas cancer with reduced survival. Cancer Cell 2014; 25: 719–734. [PubMed: 24856586]
40. Barrett R, Pure E. Cancer-associated fibroblasts: key determinants of tumor immunity and immunotherapy. Curr Opin Immunol 2020; 64: 80–87. [PubMed: 32402828]
41. Zhang Z, Chen Y, Zhang T, Guo L, Yang W, Zhang J et al. Role of Myoendothelial Gap Junctions in the Regulation of Human Coronary Artery Smooth Muscle Cell Differentiation by Laminar Shear Stress. Cell Physiol Biochem 2016; 39: 423–437. [PubMed: 27383147]
42. Gomez D, Owens GK. Smooth muscle cell phenotypic switching in atherosclerosis. Cardiovasc Res 2012; 95: 156–164. [PubMed: 22406749]
43. Biffi G, Oni TE, Spielman B, Hao Y, Elyada E, Park Y et al. IL1-Induced JAK/STAT Signaling Is Antagonized by TGFbeta to Shape CAF Heterogeneity in Pancreatic Ductal Adenocarcinoma. Cancer Discov 2019; 9: 282–301. [PubMed: 30366930]
44. Mugisho OO, Green CR, Kho DT, Zhang J, Graham ES, Acosta ML et al. The inflammasome pathway is amplified and perpetuated in an autocrine manner through connexin43 hemichannel mediated ATP release. Biochim Biophys Acta Gen Subj 2018; 1862: 385–393. [PubMed: 29158134]
45. Daley D, Mani VR, Mohan N, Akkad N, Pandian G, Savadkar S et al. NLRP3 signaling drives macrophage-induced adaptive immune suppression in pancreatic carcinoma. J Exp Med 2017; 214: 1711–1724. [PubMed: 28442553]
46. Song M, Yu X, Cui X, Zhu G, Zhao G, Chen J et al. Blockade of connexin 43 hemichannels reduces neointima formation after vascular injury by inhibiting proliferation and phenotypic modulation of smooth muscle cells. Exp Biol Med (Maywood) 2009; 234: 1192–1200. [PubMed: 19596827]
47. Provenzano PP, Cuevas C, Chang AE, Goel VK, Von Hoff DD, Hingorani SR. Enzymatic targeting of the stroma ablates physical barriers to treatment of pancreatic ductal adenocarcinoma. Cancer Cell 2012; 21: 418–429. [PubMed: 22439937]
48. Salameh A, Dhein S. Effects of mechanical forces and stretch on intercellular gap junction coupling. Biochim Biophys Acta 2013; 1828: 147–156. [PubMed: 22245380]

49. Best SA, Ding S, Kersbergen A, Dong X, Song JY, Xie Y et al. Distinct initiating events underpin the immune and metabolic heterogeneity of KRAS-mutant lung adenocarcinoma. Nat Commun 2019; 10: 4190. [PubMed: 31519898]
50. Kopp JL, von Figura G, Mayes E, Liu FF, Dubois CL, Morris JPt et al. Identification of Sox9-dependent acinar-to-ductal reprogramming as the principal mechanism for initiation of pancreatic ductal adenocarcinoma. Cancer Cell 2012; 22: 737–750. [PubMed: 23201164]
51. Yang W, Lampe PD, Kensel-Hammes P, Hesson J, Ware CB, Crisa L et al. Connexin 43 Functions as a Positive Regulator of Stem Cell Differentiation into Definitive Endoderm and Pancreatic Progenitors. iScience 2019; 19: 450–460. [PubMed: 31430690]
52. Mazur PK, Einwachter H, Lee M, Sipos B, Nakhai H, Rad R et al. Notch2 is required for progression of pancreatic intraepithelial neoplasia and development of pancreatic ductal adenocarcinoma. Proc Natl Acad Sci U S A (Research Support, Non-U.S. Gov't) 2010; 107: 13438–13443.
53. Schofield HK, Tandon M, Park MJ, Halbrook CJ, Ramakrishnan SK, Kim EC et al. Pancreatic HIF2alpha Stabilization Leads to Chronic Pancreatitis and Predisposes to Mucinous Cystic Neoplasm. Cell Mol Gastroenterol Hepatol 2018; 5: 169–185 e162. [PubMed: 29693047]
54. Izeradjene K, Combs C, Best M, Gopinathan A, Wagner A, Grady WM et al. Kras(G12D) and Smad4/Dpc4 haploinsufficiency cooperate to induce mucinous cystic neoplasms and invasive adenocarcinoma of the pancreas. Cancer Cell 2007; 11: 229–243. [PubMed: 17349581]
55. Sin WC, Aftab Q, Bechberger JF, Leung JH, Chen H, Naus CC. Astrocytes promote glioma invasion via the gap junction protein connexin43. Oncogene 2016; 35: 1504–1516. [PubMed: 26165844]
56. Zhang X, Sun Y, Wang Z, Huang Z, Li B, Fu J. Up-regulation of connexin-43 expression in bone marrow mesenchymal stem cells plays a crucial role in adhesion and migration of multiple myeloma cells. Leuk Lymphoma 2015; 56: 211–218. [PubMed: 24724781]
57. Dvorak HF. Tumors: wounds that do not heal-redux. Cancer Immunol Res 2015; 3: 1–11. [PubMed: 25568067]
58. Grek CL, Prasad GM, Viswanathan V, Armstrong DG, Gourdie RG, Ghatnekar GS. Topical administration of a connexin43-based peptide augments healing of chronic neuropathic diabetic foot ulcers: A multicenter, randomized trial. Wound Repair Regen 2015; 23: 203–212. [PubMed: 25703647]
59. Huang GY, Xie LJ, Linask KL, Zhang C, Zhao XQ, Yang Y et al. Evaluating the role of connexin43 in congenital heart disease: Screening for mutations in patients with outflow tract anomalies and the analysis of knock-in mouse models. J Cardiovasc Dis Res 2011; 2: 206–212. [PubMed: 22135478]
60. King TJ, Lampe PD. Mice deficient for the gap junction protein Connexin32 exhibit increased radiation-induced tumorigenesis associated with elevated mitogen-activated protein kinase (p44/Erk1, p42/Erk2) activation. Carcinogenesis 2004; 25: 669–680. [PubMed: 14742325]

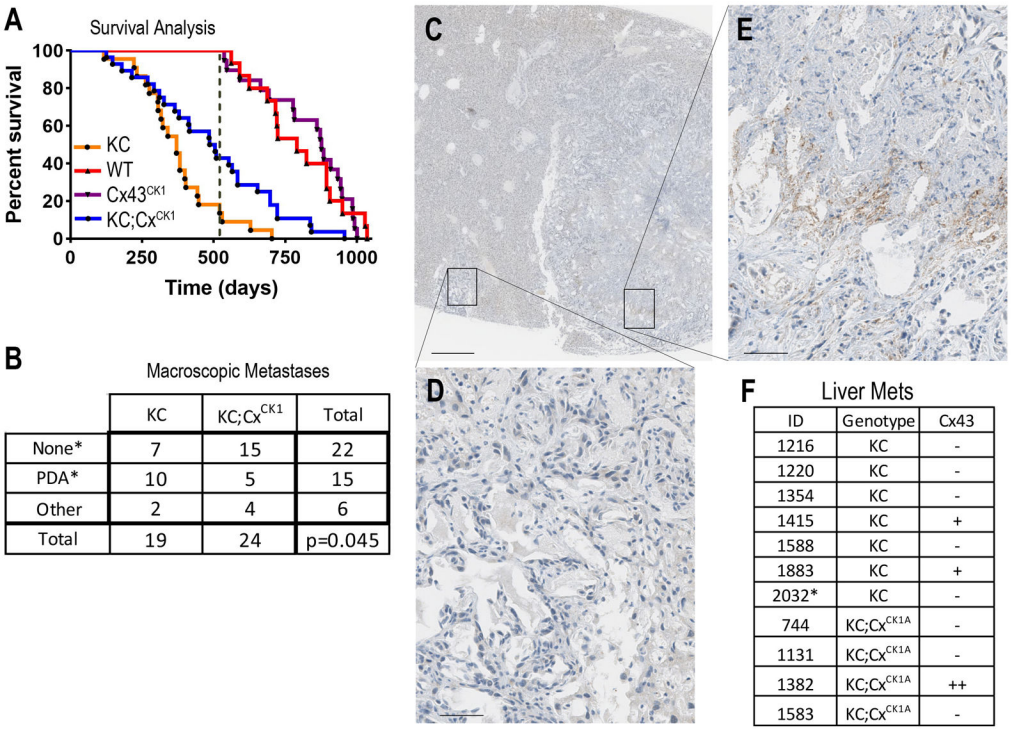

	KC	KC;Cx^{CK1}	Total
None*	7	15	22
PDA*	10	5	15
Other	2	4	6
Total	19	24	p=0.045

ID	Genotype	Cx43
1216	KC	-
1220	KC	-
1354	KC	-
1415	KC	+
1588	KC	-
1883	KC	+
2032*	KC	-
744	KC;Cx^{CK1A}	-
1131	KC;Cx^{CK1A}	-
1382	KC;Cx^{CK1A}	++
1583	KC;Cx^{CK1A}	-

Figure 1. KC;CxCK1 mice have a longer lifespan and decreased metastatic burden compared to KC mice.

(A) Kaplan Meier curves showing survival of wild type (WT), Cx43^{CK1}, KC and KC;Cx^{CK1A} animals (KC vs KC;Cx^{CK1A}, p=0.03 by log-rank). Dashed line indicates earliest death for animals without activated Kras. (B) Table shows number of animals with metastases that were visible upon necropsy and histological identification as PDA or other (non PDA derived metastasis) (*Used to determine difference in number of PDA derived metastases in KC vs. KC;Cx^{CK1} , p=0.045 by Fishers exact test). (C) Low magnification image of liver metastases from a KC animal (#1415) immunostained for Cx43 (bar is 500μm). Zoomed images show examples of Cx43 expression in a small (D) and a large (E) metastasis (bars are 50μm). (F) Table indicating amount of Cx43 expression by IHC in metastases from KC and KC;Cx^{CK1A} animals.

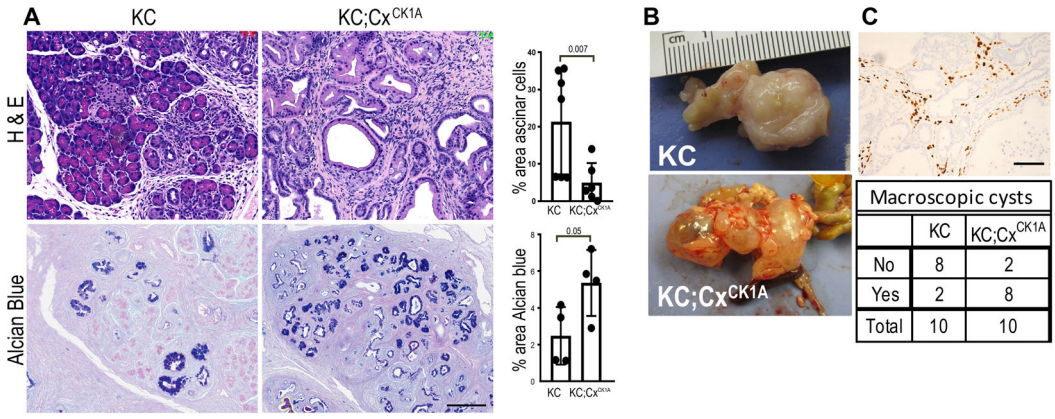

Figure 2. KC;Cx^{CK1A} mice show rapid onset of tumorigenesis and exhibit an MCN phenotype.

A) Representative H&E and Alcian blue staining of pancreata from 6-month old mice. Proportion of normal parenchyma in tissue quantified in upper graph (n=6 mice/genotype, unpaired t-test, 2-tailed). Proportion of Alcian blue staining in tissue quantified in lower graph (n=4 mice/genotype, unpaired t-test, 2-tailed). B) Images show typical tumors from 16-month old mice of both genotypes. C) IHC shows progesterone receptor staining in from a 16-month old KC;Cx^{CK1A} pancreas. Table indicates number of mice demonstrating visible cysts at necropsy (p=0.023 by Fishers exact test). Bars are 100μm.

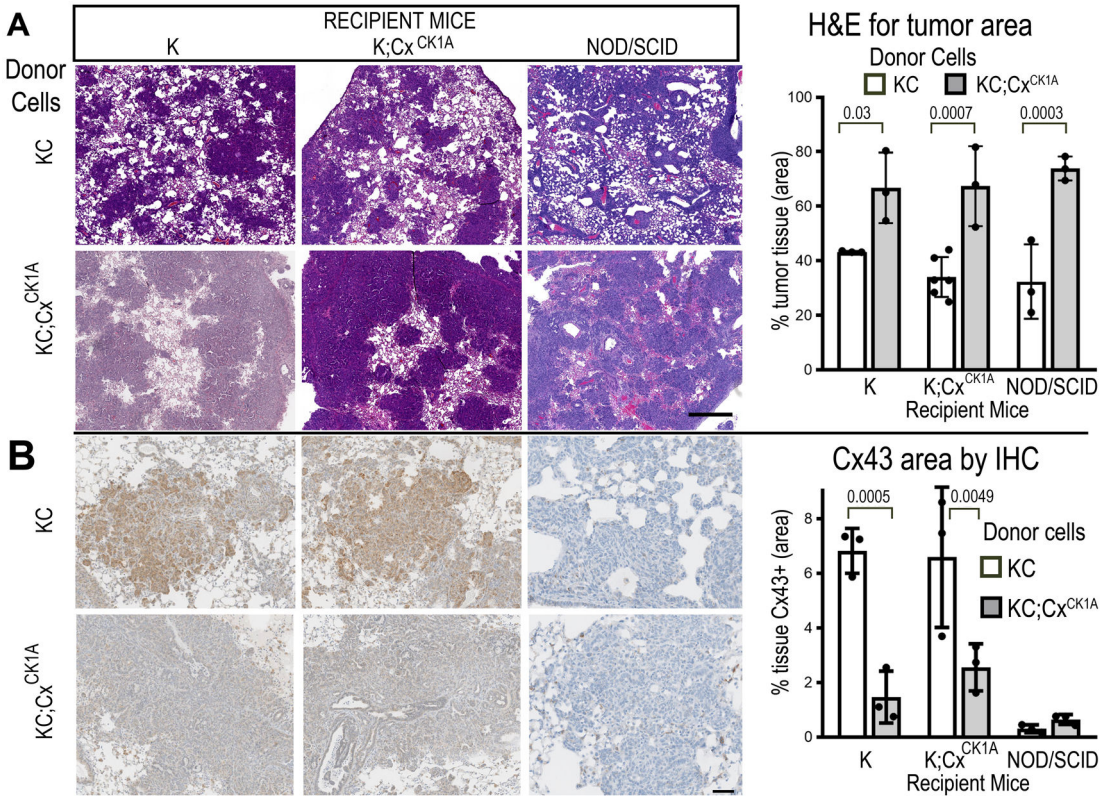

Figure 3. Cx^{CK1A} mutation does not inhibit ability of tail vein injected tumor cells to colonize the lung.

A) Representative images of mouse lungs from tail vein metastasis assay. Top panels show H&E (bar is 500μm) and bottom panels show IHC staining for Cx43 (bar is 100μm). B) Proportion of lung tissue occupied by tumor cells is quantified in upper graph and proportion of tissue staining positive for Cx43 is quantified in lower graph (n=3 mice per condition, Sidak's multiple comparisons).

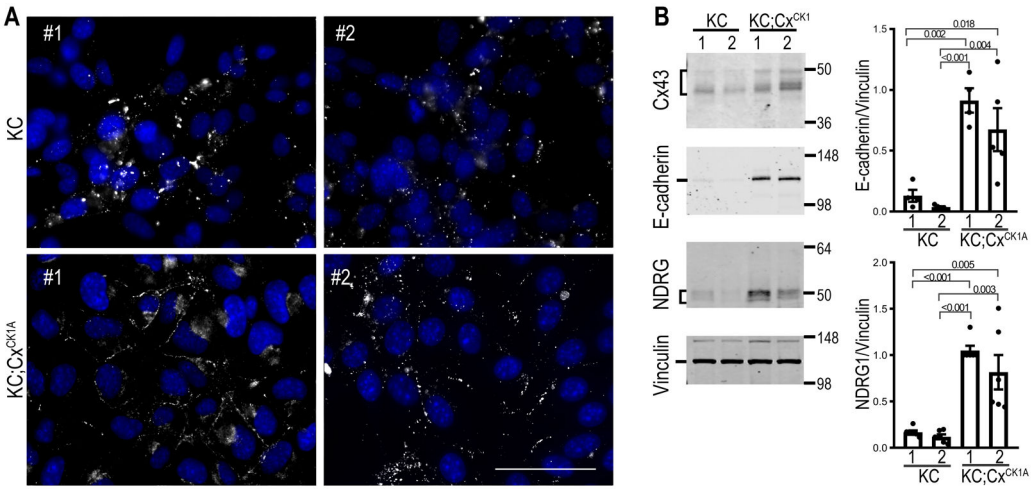

Figure 4. Cx^{CK1A} mutation promotes an epithelial phenotype.

A) Representative immunofluorescence image showing Cx43 expression in primary tumor cell lines derived from 2 different KC and KC;CxC^{K1A} pancreas tumors (1 and 2, bar is 50 μm). B) Immunoblot analysis of primary tumor cell lines showing expression of Cx43, E-Cadherin, NDRG1 and vinculin. E-cadherin, and NDRG1 levels were normalized to vinculin and quantified (n=4 experiments, Student's t-test).

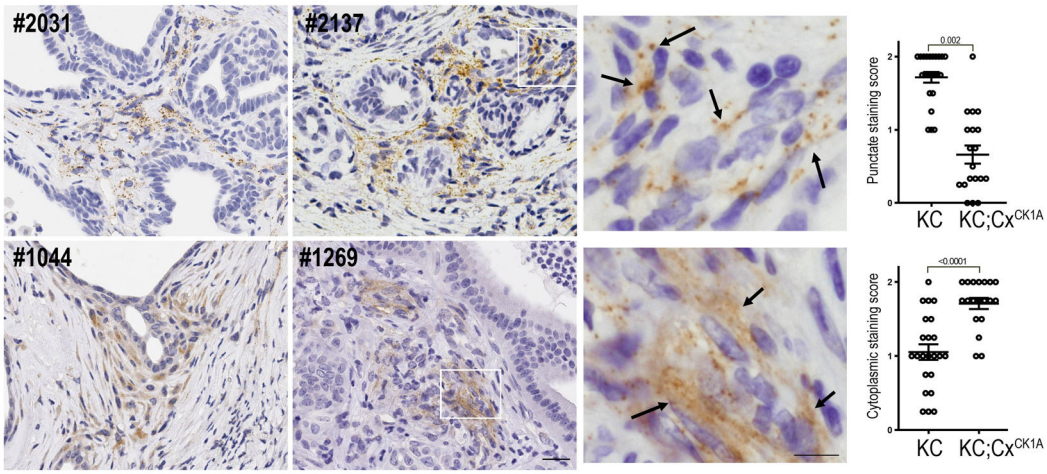

Figure 5. Gap junctions in tumor stroma are absent from KC;Cx^{CK1A} tumors.

Representative IHC staining of Cx43 in tumors from moribund mice. Arrows highlight areas with Cx43 expression. Extent of punctate staining in tissue is quantified in upper graph while extent of cytoplasmic staining is quantified in the lower graph (n=4 mice/genotype, nested t-test). Bar is 25 μm.

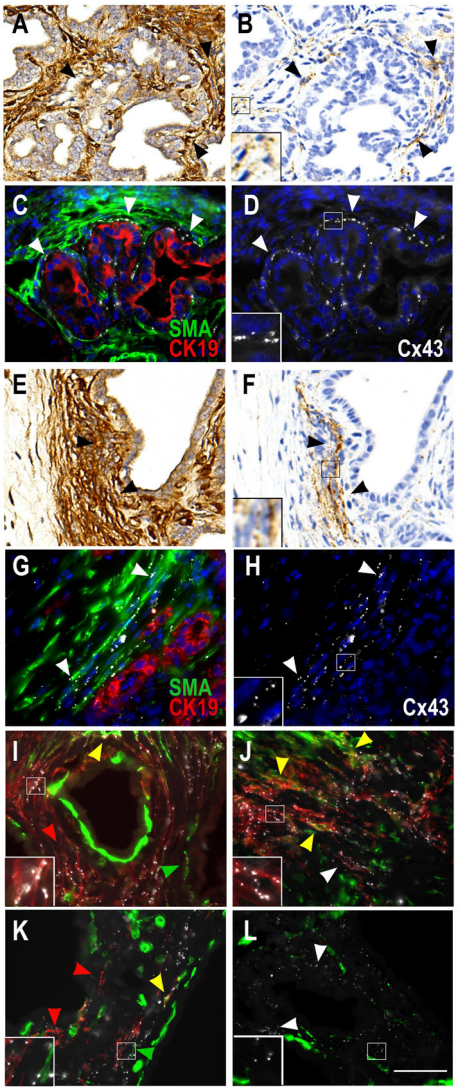

Figure 6. Cancer associated fibroblasts increase gap junction expression during tumor progression.

Representative IHC and immunofluorescence staining of invasive PDA from KC mice. Sequential sections stained for vimentin (A, E) and Cx43 (B, F) shown by IHC. Immunofluorescence images D and H show Cx43 (white) and DAPI (blue) while C and G show them overlaid with SMA (green) and CK19 (red). White arrowheads in these images point out gap junctions. Images I-L show immunofluorescence staining for Cx43 (white), SMA (green) and FAPα (red). Arrowheads in these images point out gap junctions while the colors indicate whether staining occurs in a particular cell type (red: $FAP\alpha^{+}$, green: SMA^{+}, yellow: $FAP\alpha^{+}/SMA^{+}$ and white: $FAP\alpha^{-}/SMA^{-}$). Bar is 50μm.